This is the peer reviewed version of Scott, P. and Lees, J.M. (2012) "Effects of solution exposure on the combined axial-shear behaviour of unidirectional CFRP rods" Composites Part A: Applied science and manufacturing v. 43A, (9) 1599–1611 which has been published on http://dx.doi.org/10.1016/j.compositesa.2012.03.027

Effects of solution exposure on the combined axial-shear behaviour of unidirectional CFRP rods

P. Scott[1] and J.M. Lees[2]

[1] Department of Engineering, University of Cambridge

[2] University Senior Lecturer, Department of Engineering,

University of Cambridge, Trumpington Street, Cambridge, UK CB2 1PZ

Tel: +44-(0)1223-332678, FAX: +44-(0)1223-332662,

email: jmL2@eng.cam.ac.uk (corresponding author)

Abstract

In fibre reinforced polymer (FRP) prestressed concrete applications, an FRP tendon must sustain high axial tensile stresses and, if cracks occur, additional dowel forces. The tendon may also be exposed to solutions and so the combined axial-shear stress performance after long-term environmental exposure is important. Experiments were conducted to investigate the combined axial-shear stress failure envelope for unidirectional carbon FRP tendons which had been exposed to either water, salt water or concrete pore solution at 60°C for approximately eighteen months. The underlying load resisting mechanisms were found to depend on the loading configuration, restraint effects and the initial stress state. When saturated, CFRP tendons are likely to exhibit a reduced shear stiffness. However, the ultimate limit state appeared to be fibre-dominated and was therefore less susceptible to reductions due to solution uptake effects.

Keywords: A. Carbon fibre, A. thermosetting resin, B. Environmental degradation D. Mechanical testing

[1]Present address: Cambridge Design Partnership, Cambridge, UK ps@cambridge-design.co.uk

Introduction

In prestressed concrete, the internal prestress tendons can be subjected to stresses due to dowel forces generated as a result of relative displacements across a cracked surface (see Fig. 1) [1]. Dowel action is believed to be of particular importance for the shear resistance of the structure. Fibre reinforced polymer (FRP) tendons for prestressed concrete applications will have a high volume fraction of unidirectional fibres. For an FRP tendon, dowel forces are sustained through bending, shear and contact mechanisms, however these mechanisms are compromised if the matrix fails in shear. The effectiveness of the dowel action will also be related to the width of the shear crack, i.e. the length over which the tendon sustains the dowel force, and the shear displacement, i.e. the transverse displacement caused by crack rotation. These dowel shear forces will induce a combined stress state in the tendon bridging the crack.

The Tsai-Hill failure criterion is potentially a valuable tool for predicting the limits of combined longitudinal and shear stresses that a carbon (CFRP) tendon can sustain [2, 3]. The Tsai-Hill criterion for orthotropic composites defines the combinations of stress that will cause failure as:

$$\frac{\sigma_1^{\,2}}{S_1^{\,2}} - \frac{\sigma_1\sigma_2}{S_1^{\,2}} + \frac{\sigma_2^{\,2}}{S_2^{\,2}} + \frac{\tau_{12}^{\,2}}{S_{12}^{\,2}} = 1 \qquad (1)$$

where σ_1 , σ_2 and τ_{12} are the applied axial stress, transverse stress and shear stress and S_1, S_2 and S_{12} are the axial strength, the transverse strength and the shear strength of the material respectively. Fig. 2 illustrates a typical Tsai-Hill failure envelope for a CFRP tendon with an axial failure strength of 2250 MPa, and a shear strength of 394 MPa. From Fig. 2, it can be seen that for a typical level of initial prestress say 60 %, a 33 % reduction in tendon shear strength could be expected. Therefore, the extent to which CFRP tendons can withstand shear loading at crack sites could be a determining factor in selecting the level of initial prestress.

Experimental investigations to determine the relationship between the dowel capacity and the axial tendon force in FRP prestressed concrete have been conducted. Park and Naaman [4] tested CFRP prestressed concrete beams in three point bending to assess the influence of the CFRP dowel strength on the ultimate transverse load capacity of the beams. They concluded that in many instances the failure

could be attributed to the shear load applied to the tendon across the shear crack which resulted in the rupture of the CFRP tendons. Shear loads achieved were 12 % lower than those sustained by similarly steel prestressed beams. A further series of prestressed beams [5] were designed such that the shear was transmitted entirely by a prestressing tendon. From the experimental results, it was concluded that the dowel forces were transmitted by bending, shear, and what was described as a cable effect, where increasing the prestress increased the stiffness of the shear force/shear deflection relationship. The relationship between tensile and shear forces in the tendons at failure was predicted well by the Tsai-Hill failure criterion. Shear loads achieved were 40 % of those sustained by similarly steel prestressed beams. These studies show that, compared to steel, though the shear strength values for CFRP tendons and prestressed members are lower, they are sufficient that significant dowel forces may be transmitted through CFRP tendons.

In service, FRP tendons are potentially exposed to aggressive solution environments such as the concrete pore water surrounding an embedded tendon, and salt water solutions. To predict the long-term durability of a system it is necessary to determine how the shear-axial stress interaction will change as a result of exposure. Carbon fibre-epoxy tendons are considered in the current work. Although carbon fibres are typically felt to be durable when exposed to solutions [6], epoxy matrices are susceptible to plasticisation [7]. This has implications for the matrix shear strength and fibre/matrix bond. Since dowel forces are generated at crack locations, any effects of solution uptake on the failure envelope of a CFRP tendon under axial and shear loading is therefore important. The current work describes an investigation to characterise the effect of water, salt water and concrete pore solution on the shear strength of unstressed and stressed CFRP tendons. Although prestressed concrete is the main focus, the behaviour of FRP dowels under exposed conditions is also relevant to many other applications such as pavements and connections for building facades.

Effect of uptake on CFRP strength

To assess the influence of solution uptake on CFRP mechanical properties, the durability of FRP tendons and laminates under either pure axial, or shear loading was reviewed.

Pure axial loading

The tendon axial strength is a fibre-dominated property. Graphite is chemically stable at normal temperatures and does not react with water, salts contained in sea water or alkali hydroxides found in concrete [6]. Nevertheless, Uomoto *et al.* have reported strength losses of 5 % to 8 % in individual carbon fibres after 120 days immersion in water and 1 mol/dm^3 alkali solutions [8]. Chen *et al.* [9] found a 4 % reduction in strength due to the exposure of a 9 mm diameter CFRP tendon to salt water at 60°C for 70 days. Katsuki and Uomoto [10] found the tensile strength of 6 mm diameter carbon/vinylester tendons exposed to 2 mol/litre NaOH for 120 days at 40 ^{o}C to be 4 % higher than control specimens. In such composites, axial strength reductions due to exposure are generally small and can be explained in part by the reduced effectiveness of stress transfer between fibres caused by matrix plasticisation [11].

Shear – Short beam tests

The effects of exposure on the dowel strength of CFRP tendons has not been studied extensively so reference has been made to work on laminate systems. The shear strength of FRP laminates is typically obtained using experimental set-ups such as those recommended by the American Society of Testing and Materials (e.g. [12, 13]), British Standards (e.g. [14]) etc. and is primarily assessed using short beam shear tests [13, 14]. In a short beam shear test, the loading generates combined bending and shear stresses which can obscure the desired observation of 'shear' behaviour [15]. Nevertheless, all the results reported in the following were obtained using short beam shear tests.

Carbon/epoxy laminates have been tested in a variety of conditions and, in general, the shear strength has been found to reduce with exposure to moisture and temperature. Reductions in shear strength of 20 % were noted after 121 days exposure of 2-3 mm thick laminates to 95 % relative humidity at room temperature [16] whereas exposure of laminates to boiling water for 50 days resulted in a 40 % reduction in the interlaminar shear strength (ILSS) [17]. A 58 % reduction in ILSS of a 2mm laminate was witnessed after exposure to steam for 37 days [7]. The effect of solution type on the shear strength of carbon/epoxy composites does not appear to have received a great deal of attention. However, d'Almeida [18] found exposure of 3.3 mm thick unidirectional laminates to distilled water and a salt solution analogous to sea water for 84 days at an unspecified temperature caused shear strength reductions of 38 % and 29 % respectively. The increased degradation of the distilled water specimens was attributed to the greater solution uptake observed, rather than any difference in degradation mechanism. Zhang and Mason [19] found that exposing 2.4 mm thick laminates to distilled water, synthetic sea water solution

and alkali solution (10 % NaOH) for 30 days at room temperature caused reductions of 6 %, 10 % and 27 % in the ILSS respectively.

Test method to evaluate shear strength of exposed unstressed and prestressed CFRP tendons

The aim of the current study was to test the properties of round, 4.2 mm diameter CFRP tendons to investigate the interactions between the exposure conditions and the axial and shear stress states. These results could then be extended to consider the implications for a tendon bridging a crack in a concrete environment. The selected approaches are described in the following.

Shear testing

Various standard shear strength test methods for FRP tendons were reviewed [20, 21] but double shear methods [22, 23, 24] whereby a tendon is supported from below whilst guillotined from above were considered to be the most promising. This type of test is also used to measure the shear strength of timber dowels [25] and metallic pins [26]. The method proposed by ACI Committee 440 [22], which is similar to the JSCE-E 540-1995 approach [23], was selected for further study.

The test rig based on ACI 440.3R-04 is shown schematically in Fig. 3. The rig is made from hardened steel and consists of a base with a longitudinal V-shaped cut for placing FRP samples and a central rectangular slot with an upper and two lower plates. The upper plate is used to apply the load and the lower plates are aligned to the height of the tendon. The specimen is pinned into position using the three bolts that pass through the attach plates. The shear strength, S_{12}, is calculated as the failure load, F_u, divided by twice the cross section area of the tendon. The advantages of the technique are that it is specifically designed for testing FRP tendons and has the necessary flexibility such that it can readily be included within a prestressing frame. The disadvantages are that, given the relative novelty of testing FRP bars in shear, the method has not been used and refined to same extent as some other methods. Also, the 'average' shear strength may not reflect the complexities of the shear stress distribution.

The dimensions given in the ACI-440 standard [22] were used with the exception of the plate thicknesses and the slot widths. The ACI standard was designed for larger diameter tendons so the width of the top plate was reduced from 25.4 mm (as given in the standard), to 8.4 mm to maintain a span:depth ratio of 2, which was broadly consistent with the back-calculated larger diameter tendon span:depth ratios. The

thicknesses of the lower plates were increased accordingly. The gaps between the plates and the steel base were less than 0.25 mm in accordance with the ACI test procedure. To allow for tendon surface features such as ribs and coatings, the recommended ACI slot widths are larger than necessary [27]. As the test length of the tendon was smooth, this additional space was not necessary in this investigation. The slot width was therefore chosen to be 4.5 mm, which is consistent with the back-calculated larger tendon diameter to slot width ratios stated by the ACI. A further modification was that the slot depth in the upper plate was reduced from 27.5 mm to 8 mm to facilitate measurement of tendon deflection, as described later in this section. 3 mm thick PTFE disks were glued to the bottom of the three bolts to facilitate prestressing, by minimising the friction between the bolts and the tendon.

The ACI standard specifies that the slots in the plate should have a flat surface, hereafter referred to as a 'flat' plate testing (see Fig. 3). But it was also felt that the in-concrete behaviour might be better represented by loading with plates that had less sharp edges. The use of slots with a rounded bearing profile, hereafter referred to as 'round' plate testing, then bore similarities to a short beam shear test. The dimensions of the round plates were identical to the flat plates, with the exception that each loading and support face was inscribed with a 4.2 mm fillet radius made with a ball nose (hemispherical) cutter (Fig. 3). The experimental series included both flat and round plate tests. In practice, the tendon loading due to local cracking in a prestressed concrete beam would be expected to be analogous to a situation that is somewhere in between these two test methods.

Combined axial-shear stress testing

To conduct tests under different combinations of axial and shear stress, the dowel shear test rig was bolted into a self-reacting prestress rig which was then secured to a strong floor. The prestressing tendon anchorages were aligned at the same level as the V-block supports of the dowel test rig, where the shear loading was applied. To anchor the tendons, two different systems were used, depending on the required level of axial stress. Wedge mechanical anchors supplied by SACAC were suitable for lower axial stresses (see Fig. 4(a)) whereas potted resin anchors (see Fig 4. (b, c)) were used for high stress ranges.

Exposure and uptake

The CFRP tendons consisted of unidirectional tenax UTS 5131 fibres in a Bakelite Rutapox 4539 matrix. The fibre volume fraction was 0.63. One complication was that the CFRP tendons were supplied with a

sand coating to improve the bond in concrete applications. However, for tendon sections that were to be exposed, the coating was removed by manually scraping with a sharpened edge taking care not to remove more than the coating and resin-rich surface region. This coating removal was undertaken in order to isolate the tendon uptake from that of the coating and to provide a smooth surface for shear loading. Ten measurements of the diameter at random points on a prepared tendon surface showed a standard deviation of 0.0168 mm on the diameter, indicating a negligible effect on roundness. Further details of the sand coating removal method are presented elsewhere [28].

The selected exposure conditions were water (W), salt water (SW) and concrete pore solution (CPS). Deionised water was used in all cases. The salt water consisted of 3.5 % by mass sodium chloride (NaCl) and the CPS was comprised by mass of 0.68 % sodium hydroxide (NaOH), 1.8 % potassium hydroxide (KOH) and 0.5 % calcium hydroxide $Ca(OH)_2$, having a pH of approximately 13.5, as proposed by Chin *et al.* [29]. It was noted that the $Ca(OH)_2$ added to the CPS was in excess of what could be dissolved. The concentration of $Ca(OH)_2$ was found to be much higher than that indicated in [30] but further investigations showed that even when reducing the concentration to the level reported by Christensen [30], the solution was still saturated, and some undissolved calcium hydroxide remained [31].

All the samples were from the same batch of tendons. The specimens which were not axially loaded were cut into 300 mm long lengths, stripped of sand along the entire length and placed in a sealed polypropylene container filled with the appropriate solution. Specimens to be prestressed or tested axially were cut to a 900 mm length. The central 300 mm was stripped of the sand coating and exposed to solution (see Fig. 5). The coating at the ends was left untouched to maximise the grip available to the anchorages. To accelerate the moisture uptake within a limited time period, the majority of the test specimens were exposed to solutions at 60°C by placing them in a fan oven. To assess any possible deterioration due to heating, additional temperature validation samples were exposed to 60°C but were sealed in containers without solution (referred to as 'temperature validation' samples). A further set of 'uptake validation' samples were placed in solution but stored in a temperature controlled lab at 20°C.

To estimate the solution uptake at a given time, three 150 mm long samples of the same material were fully immersed at 60°C in water, SW or CPS (see Fig. 6). Complete immersion introduces the possibility of longitudinal diffusion through the ends of the specimens. However, analytical studies [31] indicated

that these longitudinal effects should not be significant. The mass uptake readings were therefore used to infer the uptake in the axial/shear test samples at any given time. As each test series was carried out in sequence, there is some variation in the exposure period but the spread is sufficiently small that a nominal exposure time of 531 days (nominally 17.5 months) can reasonably be assumed. At this time, the uptake had departed from the initial linear relationship with the square root of time. This implies that the materials were approaching saturation, and the accelerated test conditions had achieved the objective of providing a stark contrast in uptake to control specimens.

A further three 150 mm long samples were exposed to water at 20°C in a temperature controlled lab. These were used to give a baseline mass uptake for 'uptake validation' samples where the aim was to identify that, for a given mass uptake, the same degradation could be expected regardless of whether the uptake occurred at 20°C or 60°C. The mass uptake for these 20°C specimens has been included in Fig. 6. The uptake was still in the initial stages (linear with the square root of time) which is consistent with a partially saturated concentration profile. The effect of accelerated uptake was assessed by assuming that specimens exposed to 20°C over ≈17 months have absorbed approximately equal quantities of solution at 60°C over ≈ 36 days, an observation based on the experimental mass uptake readings shown in Fig. 6.

One possible source of variability in the uptake results is the initial moisture condition. Due to time constraints, the number of specimens, and the difficulty in desiccating long specimens, the specimens were not dried before exposure. The desiccation of three typical 150 mm samples for 25 days suggested a baseline moisture content of at least 0.3 % by mass. The control specimens and the exposed specimens stored at 20°C were tested at different times of the year. Over the period of a year, the relative humidity in the lab varied between 31 and 70% but the influence of this difference is expected to be small since the percentage mass increase in three 150 mm long tendons exposed to the ambient lab environment for a 25 day period fluctuated by only 0.02 %.

Experimental testing

The pure axial capacity of the exposed and unexposed CFRP tendons was determined from an axial tensile test conducted in an Instron testing machine. The combined axial-shear test rig was used for all other selected combinations of stress and exposure.

Pure axial loading

In the pure axial tensile tests, the main variables were the exposure conditions – no exposure (C) or salt water (SW) and the exposure temperature – either 20°C (20) or 60°C (60). The axial specimens were tested using the potted anchors described previously. To prevent evaporation during potting, a polypropylene sleeve filled with the same solution was held in place over the exposed tendon region by o-rings. The sleeve was pushed to one end prior to testing. The axial tests were conducted with a 100 kN load cell and strain was measured with a laser extensometer over a gauge length of 80 mm. The crosshead rate was 0.5 mm/min.

Combined axial–shear and exposure testing

In the combined axial-shear testing the main variables were: the exposure conditions – no exposure (C), water (W), salt water (SW) or concrete pore solution (CPS); the exposure temperature – either 20°C (20) or 60°C (60); the shape of the plate slot face - flat (F) (as used in the ACI 440 method) and round (R) (with a fillet radius); the initial prestress – no prestress (0), a low initial prestress load (L) of 9.8 kN or a high prestress (H) of 19.7 kN which were chosen based on anchorage capabilities and to be as equi-spaced as possible between zero and the nominal axial failure load of 37 kN quoted by the manufacturer.

Test preparation and measurement

For the low prestressed tests, the specimens were fed through the rig and the mechanical anchors (see Fig. 4(a)) were fitted by hand at each end. Once removed from solution the specimens were tested within 15-30 mins, to minimise evaporation. For the high prestressed tests, the polypropylene sleeves used to prevent moisture evaporation from the tendons during the potting process were pushed out of the way and the tendons were anchored at each end of the prestress rig using threaded nuts (see Fig. 4(b)). The tendons were prestressed using a hydraulic jack and monitored using a 50 kN pancake loadcell.

The shear load was applied to the tendons by a hydraulic actuator fixed to the underside of a support frame above the dowel test rig. A 25 kN loadcell on the base of the actuator was free to articulate in a ball seat which was machined into an aluminium block that was used as an interface to the upper plate (see Fig. 7). The displacement of the actuator shaft was controlled and monitored with a 25 mm linear resistive displacement transducer (LRDT). The displacement of each end of unprestressed specimens with respect to the dowel test rig (slip) was measured using two 25 mm LRDTs mounted on an adjacent

scaffolding rig. All transducers were calibrated before, and rechecked after, testing. They were found to have an accuracy within 1 % of known reference loads and displacements.

To more accurately reading the tendon deflections, a transducer was positioned on the bottom of the tendons under the centre of the upper loading plate (Fig. 8). Access to this region was particularly difficult so a metal cantilever with strain gauges on the top and bottom surfaces was fixed to the side of the dowel test rig and the tip was positioned under the tendons at the centre of the gap between the lower plates. A short pointer at the end of the cantilever touched on to the bottom of the tendons. By calibrating the cantilever strains to imposed deflections, a linear displacement transducer was devised. The method offered an improved resolution and sensitivity at the start of deflection and on deflection reversal.

Testing procedure

Before each test, the plates were cleaned and sprayed with a PTFE lubricant to minimise friction. For the unprestressed tests, if the specimens had just been removed from solution, they were rinsed with deionised water and blotted dry. Specimens were promptly loaded into the test rig and the measurement devices attached. To secure the specimens the restraining bolts were tightened to a torque of 1.2 Nm.

The shear loading was applied using the hydraulic actuator, controlled using an LRDT measuring crosshead displacement data fed into a dedicated LABVIEW PC software programme. Tests were displacement controlled at a rate of 0.1 mm/minute which was found, for the flat plates, to equate to an increase in the nominal shear stress in the tendons of 30 – 60 MPa / minute, as stipulated in the ACI 440 method. A pressure relief valve ensured that the prestress was held at a steady load throughout the test. The data was logged every 0.1 seconds.

Experimental results

Pure axial loading

The average results from the pure axial tests are shown in Table 1 where C-20-100-AVE and SW-60-100-AVE correspond to the control samples tested with no exposure and stored at 20°C, and those exposed to salt water solution at 60°C, respectively. The data from one control test was lost due to a logging error, but the failure load was recorded manually. Whether failure occurred in the anchorage or the free length

is also noted. The average manufacturer's results for 13 specimens that failed in the free length, out of 30 axial strength tests, have also been included in the Table.

The axial stress/strain behaviour was fairly linear. On occasion slip at the anchorages would cause a reduction in tensile strain, which was then recovered as loading progressed further. In certain instances prior to failure, sections of the tendon would splinter at a load of around 20 to 25 kN without precipitating final failure. These splinters appeared to originate in the free length at the outer tendon surface and could be due to uneven stress transfer and/or local fibres exceeding their strength capacity. Final failure tended to be sudden and explosive, with the exception of one SW specimen where cracks occurred over a period of five seconds. Significantly, two of the three exposed specimens failed in the tendon free length (see Fig. 9(a)) whereas all four control specimens (see Fig. 9(b)) failed in the anchorages. This could be an indication of degradation of axial strength caused by exposure to salt water solution.

The measured axial strengths were lower than those reported by the manufacturer, but since the failure of the control specimens originated in the anchorages, the true axial strengths will be higher than measured. The average SW specimen axial strengths were 9 % lower than those of the control specimens. As the failures were mostly in the free length, the failure strengths should be closer to the true strengths. The reduction in axial strength due to salt water exposure could be due to the reduced effectiveness of the degraded matrix to re-distribute loads in shear lag regions around lower strength fibres.

Dowel testing - shear and combined axial-shear testing

A total of 78 dowel tests were conducted to explore the interactions between the tendon axial stress, the shear stress and exposure. One observation was that, in the tests with prestress it was noted that even with a pressure relief valve at the live jacking end to maintain a constant prestress, in certain instances, the measured prestress increased during the test. This was attributed to the frictional stresses generated between the live end and the loadcell at the dead end of the tendon. As a result, the axial stress in the loadcell end of the tendon was on occasion up to 5% higher than that in the jacking end of the tendon, and up to 10% higher in certain tests of exposed specimens using round plates at low prestress.

The flat and round plate test results are shown in Tables 2 and 3 respectively. The shear stresses at failure are calculated as the applied shear load divided by twice the cross section area and the axial stress at

failure was based on the load cell reading. To ascertain the tendon area, the tendon diameter was measured in 5 places using a micrometer before exposure. Across the specimens the standard deviation in cross section areas was 0.10mm^2, giving a COV of 0.0074 mm^2. The percentage mass increase in each specimen at the time of testing was calculated from its exposure period and interpolation of the uptake data in Fig. 6. The notation used to identify each specimen (AA-B-C-D-E) is shown in the Table legends where, for example, test C-20-F-0-1 corresponds to control sample #1 with no exposure, stored at 20°C, tested using flat plates and with no prestress. Specimens tested as part of the uptake validation are denoted with an asterix (*).

Results of flat plate dowel tests

Plots of load against deflection for flat plate tests with no prestress, low prestress and high prestress are shown in Fig. 10. In some no prestress tests (W-60-F-0-3, SW-60-F-0-3, CPS-60-F-0-1,2,3), the failed specimens continued to support a small amount of shear load, and so had to be unloaded. In all the other tests, the shear load dropped to zero after failure. The key results are shown in Table 2. Typically three specimens for each set of parameters were tested so where more than one specimen was tested, an average (mean) value and two times the standard deviation are indicated.

Figure 10 and Table 2 show that, regardless of the solution, exposure has a relatively small effect on the ultimate shear load, causing a reduction in the order of 10-15 % compared to control specimens. The solution is seen to have an effect on the load/deflection stiffness which is particularly evident in Fig. 10(a) and the associated expanded view in Fig. 10(b). These figures show that exposure to water or SW solution causes an appreciable decrease in stiffness, and exposure to CPS causes an even greater reduction. As the ultimate transverse load strength does not appear to be significantly affected by exposure, it may be hypothesised that the ultimate failure mechanism in the flat plate tests is not matrix-dominated, but fibre-dominated. This would imply that as the prestress load increases, the transverse loads and deflections that can be sustained by the tendons should decrease. This is consistent with the results in Table 2 where, for a given exposure condition, the maximum shear stress sustained by the tendons with a high prestress were between 30 and 39% lower than the equivalent unstressed results.

Results of round plate dowel tests

Plots of load against deflection for round plate tests with no prestress, low prestress and high prestress are shown in Fig. 11. The round plate test behaviour differs markedly depending on whether or not the specimens were prestressed. This was attributed to differences in the tendon restraint. Slip of material into the span length observed in the unprestressed tests would not occur as readily in the prestressed tests given the resistive action of the end anchors. The main results, including average (mean) values and standard deviations, are presented in Table 3. With one exception (SW-60-R-H-2), the shear load dropped to zero after the specimens failed.

Solution uptake can be seen to affect the behaviour of the specimens. In the tests with no prestress, the initial load/deflection behaviour of specimens decreases in stiffness when exposed to water or SW. This effect is even more pronounced on exposure to CPS, indicating a significant role is played by matrix shear in the round plate tests (see Figs 11(a) and (b)). This hypothesis is supported by the correlation between exposure and the load at which the initial load/deflection slope changes, denoted as the 'delamination shear stress' (calculated at the tendon centroid) in Table 3, an indication that shear failure occurs early on. Exposure appears to cause around a 10 %, reduction in the ultimate shear load sustained by the unprestressed specimens. This is less than would be expected for a purely matrix dominated failure mechanism, but does suggest that exposure has a small degree of influence.

In the low prestress tests, exposure is seen to significantly increase the transverse loads (by between 1.7 and 3.2 times) and deflections that can be sustained (Fig. 11(c) and Table 3). The stiffness at this prestress level is only initially reduced by exposure effects, suggesting that initial delamination effects are likely to be followed by fibre dominated mechanisms. At higher prestress loads, the exposed shear strengths were similar to the unexposed specimens which suggests that fibre dominated effects are responsible for failure at higher prestress levels.

The axial loading and boundary conditions have a drastic effect on the load/deflection behaviour exhibited in round plate tests, which differ depending on whether slip is allowed to occur and the level of prestress applied to the specimens. After delamination occurs within the test region, the fibers rotate and sustain further loading in tension. The lengths of tendon beyond the bolt clamps act to prevent further delamination growth and remain intact. Hence, when prestressed, they provide additional restraint to the tendon within the test region.

Additional Validation tests

As discussed, additional tests were conducted to confirm that the accelerated testing had no adverse effects on the behaviour. Though presented elsewhere [31], in summary the plots of load against deflection in the temperature and uptake validation tests showed similar trends as noted previously in the tests using either flat or round plates. The temperature validation results (C-20-F-0-1,2,3 vs C-60-F-0-1,2,3 and C-20-R-0-1,2,3 vs C-60-R-0-1,2,3) in Tables 2 and 3 indicate that no appreciable differences in tendon performance were caused by prolonged exposure to 60°C temperatures. The slight increases in delamination shear stress (see Table 3) as a result of heating were thought to be due to a lower moisture content in the specimens exposed at 60°C, due to evaporation effects. The results for the uptake validation tests are also presented in Tables 2 and 3. The mass uptake at 20°C in water (see Fig. 6) was used to infer the uptake in salt water and CPS using relationships described elsewhere [31]. Although only a single specimen for each comparison was tested, it appeared that the temperature had no significant effect on the degradation except that the round plate delamination shear stresses for the 60°C exposure were slightly lower. This result gives further confidence that accelerating uptake at a temperature of 60°C simulated the uptake effects that would take years to occur at room temperature. However, one significant finding that emerged was the dependency of the round plate delamination shear stress results for the CPS and, to a lesser extent, the water results on the estimated uptake. The delamination stress of the CPS-60-R-0-1* specimen result was over twice that of the average of CPS-60-R-0-1,2,3. This suggests that an increased level of solution uptake is connected with a reduction in the observed delamination stress.

SEM and optical imaging

The behaviour of specimens undergoing the ACI test with flat or round plates is complex and the notion of an average shear strength is misleading. Partial loading tests on unstressed, unexposed samples accompanied by SEM images and optical images were undertaken to help visualise the damage sustained by the specimens during loading. Four unprestressed specimens were partially loaded using flat plates and then unloaded, and a further five unprestressed specimens were partially loaded using round plates and unloaded. Selected SEM results corresponding to a load-unload loop of 2.9 kN, 5.9 kN and 7.6 kN for the flat plates and a load of 1.7 kN and a deflection of 0.7 mm, a load of 1.7 kN and a deflection of 3 mm, and a load of 16.1 kN for the round plates are shown in Fig. 12. Optical images of slices through the

tendon section in the 7.6 kN flat plate and the 16.1 kN round plate samples are also included. The corresponding load deflection curves are shown in Fig. 13. These results will be discussed in more detail in the next section.

Discussion

Using the experimental results, the relationship between nominal maximum shear stress and axial stress at failure for the various exposure conditions has been plotted in Fig. 14. A Tsai-Hill type relationship (Eqn 1) has been plotted in this figure for the control and salt water exposed specimens tested using flat or round plates. The pure axial experimental failure stresses were used as S_1, S_{12} came from the unprestressed test results. The S_2 term in Eqn 1 is assumed to be zero given the nominal absence of transverse loading on the shear plane but in practice this term may well be non-zero.

In the flat plate tests, shown as squares in Fig. 14, increases in prestress result in a decrease in shear loading that can be sustained by the tendons, as predicted by the Tsai-Hill failure criterion. The effect of exposure appears minimal however, suggesting failure is fibre dominated rather than matrix dominated. Regarding the unprestressed round plate tests, shown as circles in Fig. 14, the transverse shear load sustained is substantially higher than that of the flat plates, suggesting a significant difference between the failure mechanisms. A surprising result is found in the round plate low prestress tests, where both a great deal of scatter, and a strong dependency on the exposure conditions, were noted and in a few of the exposed specimens the shear loads and deflections were higher than the unstressed results. At high prestress, the round plate results appear to converge with the flat plate results and are characterised by lower sustained transverse loads and no exposure dependency. This suggests that loading geometry becomes less significant as the pre-load in the tendons approaches the tensile capacity. These results show caution must be exercised when considering a failure envelope based on knowledge of tensile strength and shear strength data from test methods such as those presented here. A particular limitation is that the flat and round plate tests do not provide a ‘pure’ measurement of the shear strength. The tests inherently reflect a combined stress state and, as will be discussed in the following paragraphs, a variety of different failure modes were seen within the material, prior to the ultimate failure of the composite.

Flat plate

From the flat plate unprestressed tests and images, generally it appears that matrix dominated behaviour governs the earlier part of the test behaviour, and fibre dominated mechanisms govern the latter part. Shear and bending effects are present up until the time at which initial interlaminar failures occur. Compression and bearing stresses also play a role. The SEM images of the flat plate tests (Fig. 12 (b) and (c)) show the portion of the tendon under the upper plate is effectively punched from the material supported by the lower plates. As deflections increase, fibres in the un-failed portion of the tendon are increasingly rotated causing an increased resistance to further deformation through axial strain (see Fig. 12 (d)). Ultimately, final failure tended to be brittle, indicative of a final core of fibres failing in axial tension having undergone a significant amount of rotation. Inspection of the failure surfaces showed evidence of shearing and scraping at the top and bottom of the section, with a cleaner break in the central region. One outcome is that although the test method has been designed to evaluate shear strength, it ultimately appears to measure a tensile fibre rupture mechanism. The effect of exposure on the ultimate capacity of the unprestressed samples is small. A reduction in initial load/deflection behaviour is observed when matrix effects are dominant, but little degradation of ultimate strength is witnessed, as fibre dominated effects appear to govern ultimate behaviour.

Figs. 10(c) and (d) show that the load/deflection behaviour stiffens with increasing prestress, an expected effect caused by the restorative action of the tensile axial loading. The peak loads decrease with increasing prestress, which may be attributed to the reduced residual tensile capacity of the specimens. There appear to be no significant synergistic effects occurring due to combined prestress and exposure conditions. This further suggests that an exposure insensitive tensile failure rather than shear or compressive failure is the dominant mechanism in precipitating the ultimate limit state.

Round plate

The load deflection behaviour for the unstressed round plate tests can be split into three distinct phases, illustrated in Fig. 13(b). The SEM images of the unstressed round plate tests (Fig. 12 (e)) show that in the first phase, initial bending, shear and plastic deformation occurs on the tendon surface in regions that have been in contact with the round plates. The onset of a second phase of behaviour has been shown in previous work to be associated with interlaminar shear failures [31]. The load at which initial delamination occurs will be connected to the matrix shear strength and differences due to the exposure conditions were noted. With increasing deflection, sequential delamination failures throughout the

section are associated with a loss of stiffness which is notable as a plateau in the load-deflection behaviour. By the end of the load/deflection plateau (Fig. 12 (f)), longitudinal cracks are evident throughout the cross section. Of interest is that damage appears to be curtailed in a compressive region directly under the top plate. The large accumulated deflections lead to a situation where the change in geometry reduces the gap between the upper and lower loading plates and the tendon becomes compressed between the top and bottom plates (phase 3 behaviour). Local combined stresses in the compressed regions can potentially exceed the transverse compressive strength, resulting in local failure. The ultimate failure of the tendon is then due to an accumulation of damage through the section which at later stages is associated with axial failure of the fibres, when the unfailed proportion of the tendon becomes sufficiently small. This complex failure is believed to be inherent in the unstressed round plate experimental setup. In practice although the concrete cover will be significantly less stiff than the steel test rig, it may still exert a significant pinching effect on the CFRP tendons.

In the absence of partial loading results, for the prestressed round plate specimens it is postulated that the initial phase one bending, shear and contact behaviour appear to be similar. However, in the prestressed tendons, because slip could not occur to the same degree and the prestress stiffened the tendon, the shear load sustained rises above the load at which interlaminar shear failures occur. As the extent of delamination increases, the load supported by the tendon continues to increase and the tendon starts to behave as a cable. Although the ultimate failure is then a fibre dominated mechanism, the low prestress tests suggest that exposure may facilitate a greater flexibility and evenness of stress distribution across the tendon section by means of reduced matrix shear strength and stiffness, earlier and more numerous delaminations, matrix softening, and perhaps even reduced friction between delaminations. The absence of this phenomenon in the equivalent flat plate tests is likely explained by the plates constraining the tendons to a greater degree, by means of a shorter span length and greater contact area, preventing a cable mechanism from developing. This effect is also less pronounced at high prestress due to the lower residual tensile capacity of the tendons at the onset of shear loading. The higher tensile stresses in the tendons may interact with the transverse compressive stresses and frictional shear stresses to cause a local failure under the point load. The remainder of the tendon cross section then fails in tension.

Implications for dowel effects

The effect of degradation on the load/deflection behaviour and ultimate failure has been shown to be strongly dependent on the boundary conditions including the plate geometry, allowance of slip and prestress load. The flat and round plates bound the likely behaviour in practice. Cracks in prestressed concrete are likely to be wider than the flat plate test set-up, and narrower than the round plate set-up.
Neither test method gives a "pure" measurement of shear strength. The flat plate tests were more repeatable and gave an indication of reductions in matrix stiffness. Although the boundary conditions of the round plate tests were closer to what might be expected across a crack in a prestressed concrete structure, there was a greater variation in the results and a strong dependency on the level of initial prestress. Further work is required to establish the most appropriate test method.

In the experiments reported here, the tested sections were completely submersed in solution. In contrast, at a crack site, the moisture uptake rate and profile across and along the tendon will depend on many other factors such as the moisture availability and the concrete properties. A further consideration was that the outer sand coating was stripped from the tendon prior to exposure which could affect the tendon diffusion properties and, as a consequence, the response to axial-shear loading. More generally, the resin characteristics will play a role and, for example, the specification of a resin with a high shear strength and cross link density would increase the shear strength and stiffness of the tendons.

It is nevertheless possible to infer that it is likely that uptake induced degradation will result in a reduction in tendon shear stiffness. Therefore, CFRP tendons at shear cracks are likely to exhibit a reduced shear stiffness and suffer delamination-type shear failures at lower shear loads as they become saturated due to water, salt water or concrete pore solution exposure. CPS was found to be the most aggressive of all the solutions considered. Hence, the serviceability limit state is expected to be dominated by the matrix behaviour, but the loss in shear stiffness due to exposure is offset by evidence that the ultimate limit state is a fibre dominated mechanism and therefore less susceptible to uptake effects. In some cases, the ultimate loads and deflections that can be sustained may even increase given the increased compliance of the matrix and the ability to sustain higher shear loads in tension through cable mechanisms.

Further studies are required to more fully assess how the observed mechanisms in isolated tendons will influence the behaviour of a prestressed concrete structure. The dowel contribution from the FRP tendon to the shear performance of a concrete member may initially be small, but will then increase as shear

cracks grow and the tendon rotates, becoming axially loaded. The concrete mix, the concrete cover and internal stirrups will influence the local conditions and have been found elsewhere to have an impact on the overall behaviour [4], [5].

Conclusions

The relationship between axial stress, shear stress and the exposure conditions has been investigated in CFRP tendons. Under tensile axial loading conditions, exposure to salt water could result in an 8 % reduction in the axial tendon strength relative to unexposed control samples. Salt water specimens failed in the free length but anchorage failures in the control specimens may have artificially reduced their measured strengths. Under combined axial and shear loading, the failure mechanisms and the load/deflection behaviour can differ considerably depending on the loading configuration, restraint effects and initial stress states. Testing of CFRP tendons in double shear with flat faced plates showed that the only significant effect of exposure to water, salt water or CPS was a reduction in load/deflection stiffness during the earlier part of testing. With increasing prestress, the ultimate transverse loads and deflections sustained by the tendons reduced. Testing with rounded plates effectively tested the tendons in a short beam shear-like manner. Delamination-type shear failures parallel to the fibre direction were noted in the initial stages of loading and the onset of these failures was found to depend on the exposure conditions. In the samples with no prestress, the tendons were compressed between the upper and lower plates at large deformations. In contrast, the behaviour of the prestressed tendons was more cable-like. The ultimate loads and deflections that could be sustained at low prestress levels increased with exposure. At higher levels of prestress, the failure did not depend on the exposure conditions but the shear load and deflection capacities reduced due to the lower residual tensile strain capacity.

In practice, CFRP tendons at shear cracks are likely to exhibit a reduced shear stiffness and suffer delamination-type shear failures at lower shear loads as they become saturated. However, the ultimate limit state is likely to be a fibre-dominated mechanism and therefore less susceptible to uptake effects which, in certain circumstances, may even be beneficial.

Acknowledgements

The authors are most grateful for the support of SACAC Ltd and to Dr Giovanni Terrasi from EMPA and Dr Michael Sutcliffe from the University of Cambridge for their technical advice and input. The first

author was funded by an EPSRC DTA award which is gratefully acknowledged. The contributions of Mr Martin Touhey and Mr Si Holder from the University of Cambridge are also gratefully acknowledged.

References

1 Paulay, T., Park, R., and Phillips, M.H., Horizontal Construction Joints in Cast In Place Reinforced Concrete. *Shear in Reinforced Concrete: ACI Special Publication,* 1974. **42**(2): p. 599-616.

2 Hull, D. and Clyne, T.W., *Introduction to composite materials.* 2 ed. 2004, Cambridge, UK: Cambridge University Press.

3 Daniel, I.M. and Ishai, O., *Engineering Mechanics of Composite Materials.* 1994, Oxford: Oxford University Press.

4 Park, S.Y.P. and Naaman, A.E., *Shear Behaviour of Concrete Beams Prestressed with FRP Tendons.* Prestressed Concrete Institute Journal, 1999. **44**(1): p. 74-85.

5 Park, S.Y. and Naaman, A.E., *Dowel Behaviour of Tensioned Fibre Reinforced Polymer (FRP) Tendons.* ACI Structural Journal, 1999. **96**(5): p. 799-806.

6 Mantell, C.L., *Carbon and Graphite Handbook*. 1968, New York: John Wiley & Sons.

7. Adams, R.D. and Singh, M.M., *The Dynamic Properties of Fibre-Reinforced Polymers Exposed to Hot, Wet Conditions.* Composites Science and Technology, 1996. **56**(8): p. 977-997.

8 Uomoto, T. and Nishimura, T. *Deterioration of aramid, glass and carbon fibres due to alkali, acid and water in different temperatures,* in *Fourth International Symposium on Fibre Reinforced Polymer for Reinforced Concrete Structures*. 1999. Michigan: American Concrete Institute. p. 515-522.

9 Chen, Y., Davalos, J.F., Ray, I., and Kim, H.-Y., *Accelerated aging tests for evaluations of durability performance of FRP reinforcing bars for concrete structures.* Composite Structures, 2007. **78**(1): p. 101-111.

10 Katsuki, F. and Uomoto, T. *Prediction of deterioration of FRP rods due to alkali attack* in *Second International RILEM Symposium, (FRPRCS-2)*. 1995. Ghent, Belgium: E&F Spon. p. 82-89.

11 Rosen, B. Walter, Zweben, Carl H., *Tensile failure criteria for fiber composite materials.* NASA Contractor Report 2057, August 1972.

12 ASTM, *D 4255/D 4255M-01, Standard Test Method for In-Plane Shear Properties of Polymer Matrix Composite Materials by the Rail Shear Method*. 2002, ASTM Intl: West Conshohocken, PA. p. 156-168.

13 ASTM, *D 2344/D 2344M-00e, Standard Test Method for Short-Beam Shear Strength of Polymer Matrix Composite Materials and Their Laminates*. 2000, ASTM Intl: West Conshohocken, PA. p. 47-54.

14 British Standards Institution, *EN 2563:1997, Carbon fibre reinforced plastics. Unidirectional laminates. Determination of the apparent interlaminar shear strength*. 1997, BSI: London, UK.

15 Adams, D.F. and Lewis, E.Q., *Experimental assessment of four composite material shear test methods*. Journal of Testing & Evaluation, 1997. **25**(2): p. 174-181.

16 Gibbins, M. N. and Hoffman, D. J., *Environmental Exposure Effects on Composite Materials for Commercial Aircraft*, NASA Contractor Report 3502, January 1982.

17 Joshi, O.K., *The effect of moisture on the shear properties of carbon fibre composites.* Composites, 1983. **14**(3): p. 196-200.

18 d'Almeida, J.R.M., *Effects of distilled water and saline solution on the interlaminar shear strength of an aramid/epoxy composite.* Composites, 1991. **22**(6): p. 448-450.

19 Zhang, M. and Mason, S.E., *Effects of contamination on the mechanical properties of carbon fibre reinforced epoxy composite materials.* J of Composite Materials, 1999. **33**(14): p. 1363-1374.

20 ASTM, *D 3914-84, Standard Test Method for Apparent Horizontal Shear Strength of Pultruded Reinforced Plastic Rods by the Short-Beam Method*. 1985, ASTM Intl: West Conshohocken, PA.

21 BSI, *BS ISO 3597-4:2003, Textile-glass-reinforced plastics. Determination of mechanical properties on rods made of roving-reinforced resin. Determination of apparent interlaminar shear strength*. 2003, BSI: London, UK.

22 ACI, *ACI 440.3R-04, Guide Test Methods for Fiber-Reinforced Polymers (FRPs) for Reinforcing or Strengthening Concrete Structures*. 2004, ACI: Farmington Hills, Michigan.

23 Machida, A., ed. *Recommendation for Design and Construction of Concrete Structures using Continuous Fiber Reinforcing Materials*. 1997, Research Committee on Continuous Fiber Reinforcing Materials, Japan Society of Civil Engineers: Tokyo.

24 ISO, *Fibre-reinforced polymer (FRP) reinforcement of concrete - Test methods - Part 1: FRP bars and grids*. 2008, ISO: Geneva.

25 Eckelman, C.A. and Haviarova, E., *Load capacity and deflection characteristics of large wooden dowels loaded in double shear*. Forest Products Journal, 2007. **57**(5): p. 60-64.

26 BSI, *EN 28749 : 1992, Pins and grooved pins - Shear test*. 1992, BSI: London, UK.

27 Benmokrane, B., *RE: Transverse shear test for FRP bars*, email to the authors, 18 July 2008.

28 Scott, P. and Lees, J.M. Uptake induced swelling and thermal expansion of CFRP tendons *Structures and Buildings, Procs of the Institution of Civil Engineers* 2009 v. 162 (4) pp. 263-273

29 Chin, J.W., Nguyen, T., and Aouadi, K., *Sorption and Diffusion of Water, Salt Water and Concrete Pore Solution in Composite Matrices*. J of Applied Polymer Science, 1999. 71(3): p. 483-492.

30 Christensen, B.J., Mason, T.O., and Jennings, H.M., *Influence of silica fume on the early hydration of Portland cements using impedance spectroscopy*. J of the American Ceramic Society, 1992. 75(4): p. 939-945.

31 Scott, P. *Aspects of CFRP Prestressed Concrete Durability in the Marine Environment*, University of Cambridge, 2009. PhD Thesis

Table 1. Axial strength test results

Sample	Average area (mm^2)	Gauge length (mm)	Failure load (kN)	Axial strength (MPa)	Failure strain** (%)	Nominal modulus * (GPa)	Failure location
C-20-100-AV	13.51	83.1	29.4	2175	1.53	140.4	Anchor
SW-60-100-AV	13.59	80.0	27.0	1986	1.44	138.5	2 in free length 1 in anchor/free
Manufacturer data: Averages for failures				2733	1.62	163.0	Free length
Relative ratios of				Axial strength	Failure strain	Nominal modulus	
C-100-AV/Manufacturer free length results				0.80	0.95	0.86	
SW-100-AV / C-100-AV				0.91	0.94	0.99	

* calculated between stresses of 650 MPa and 1350 MPa
** Failure strength divided by nominal modulus

Table 2. Average results from dowel tests using flat plates

	Area (mm^2)	SQRT Days exposed	Est. uptake (%)	Axial stress at failure (MPa)		Max shear stress (MPa)		Effect of axial stress ratio	Max shear stress/ C-20-F
Specimens	Ave	Ave	Ave	Ave	2 x STD DEV	Ave	2 x STD DEV		for a given prestress
C-20-F-0-1,2,3	13.51	N/A	N/A	0	N/A	280	13.7	1	1
W-60-F-0-1,2,3	13.53	23.2	0.859	0	N/A	284	7.3	1	1.01
SW-60-F-0-1,2,3	13.51	22.77	0.789	0	N/A	269	10.4	1	0.96
CPS-60-F-0-1,2,3	13.59	23.28	0.931	0	N/A	261	11.7	1	0.93
C-20-F-L-1,2,3	13.58	N/A	N/A	709	11.3	224	34.9	0.8	1
W-60-F-L-1,2	13.62	23.81	0.871	648	130.6	184	16.5	0.65	0.82
SW-60-F-L-1,2,3	13.53	22.41	0.782	710	18.2	198	13.3	0.74	0.88
CPS-60-F-L-1	13.57	23.77	0.943	704	N/A	198	N/A	0.76	0.88
C-60-F-H-1,2,3	13.47	N/A	N/A	1452	4.8	195	28.2	0.70	1
W-60-F-H-1,2,3	13.52	23.40	0.863	1439	20.2	174	15.1	0.61	0.89
SW-60-F-H-1,2,3	13.60	23.29	0.799	1437	6.8	184	21.4	0.68	0.94
CPS-60-F-H-1,2	13.54	23.45	0.935	1439	7.6	167	25.0	0.64	0.86
C-60-F-0-1,2,3	13.63	23.73	N/A	0	N/A	303	12.9	N/A	N/A
W-20-F-0-1*	13.68	23.66	0.443	0	N/A	291	N/A		
W-60-F-0-1*	13.54	5.74	0.425	0	N/A	283	N/A		
SW-20-F-0-1*	13.53	23.73	0.415	0	N/A	288	N/A	Uptake Validation	
SW-60-F-0-1*	13.58	5.92	0.406	0	N/A	283	N/A		
CPS-20-F-0-1*	13.54	23.66	0.445	0	N/A	282	N/A		
CPS-60-F-0-1*	13.36	5.74	0.432	0	N/A	284	N/A		

LEGEND: AA-B-C-D-E

- AA: Exposure — C = control (no exposure), W = water exposure, SW = salt water exposure, CPS = CPS exposure
- B: Temperature of exposure
- C: Plate geometry — F = flat plate, R = round plate
- D: Prestress — 0 = no prestress, L = low prestress (9.8 kN), H = high prestress (19.7 kN)
- E: Sample # — 1 = first sample, 2 = second sample, 3 = third sample, 1*=uptake validation specimen

Table 3. Average results from dowel tests using round plates

	Area (mm^2)	SQRT Days exposed	Est. uptake (%)	Delamination shear stress (MPa)		Axial stress at failure (MPa)		Max shear stress (MPa)		Effect of axial stress ratio	Max shear stress/ C-20-R
Specimens	Ave	Ave	Ave	Ave	2 x STD DEV	Ave	2 x STD DEV	Ave	2 x STD DEV		for a given pre-stress
C-20-R-0-1,2,3	13.62	N/A	N/A	75.1	6.2	0	N/A	614	32.3	1	1
W-60-R-0-1,2,3	13.53	23.19	0.859	56.3	1.8	0	N/A	569	76.3	1	0.93
SW-60-R-0-1,2,3	13.55	22.82	0.790	54.8	3.7	0	N/A	577	93.5	1	0.94
CPS-60-R-0-1,2,3	13.59	23.28	0.931	32.8	4.4	0	N/A	537	17.1	1	0.87
C-20-R-L-1,2,3	13.62	N/A	N/A	N/A	N/A	710	108.5	224	71.1	0.36	1
W-60-R-L-1	13.70	24.50	0.883	N/A	N/A	813	N/A	475	N/A	0.83	2.12
SW-60-R-L-1,2,3	13.52	22.90	0.791	N/A	N/A	808	41.0	383	125.9	0.66	1.71
CPS-60-R-L-1,2	13.57	24.14	0.95	N/A	N/A	869	3	725	10.3	1.35	3.24
C-20-R-H-1,2,3	13.49	N/A	N/A	N/A	N/A	1459	26.6	161	16.7	0.26	1
SW-60-R-H-1,2,3	13.52	23.34	0.800	N/A	N/A	1455	33.1	167	15.8	0.29	1.04
CPS-60-R-H-1	13.58	23.30	0.931	N/A	N/A	1465	N/A	184	N/A	0.34	1.14
C-60-R-0-1,2,3	13.63	23.73	N/A	80.4	5.1	0	N/A	605	20.0	N/A	N/A
W-20-R-0-1*	13.68	23.66	0.443	70.2	N/A	0	N/A	555	N/A	Uptake Valid-ation	
W-60-R-0-1*	13.54	5.74	0.425	63.9	N/A	0	N/A	575	N/A		
SW-20-R-0-1*	13.53	23.73	0.415	75.1	N/A	0	N/A	601	N/A		
SW-60-R-0-1*	13.58	5.92	0.406	56.4	N/A	0	N/A	586	N/A		
CPS-20-R-0-1*	13.54	23.66	0.445	71.4	N/A	0	N/A	590	N/A		
CPS-60-R-0-1*	13.36	5.74	0.432	68.7	N/A	0	N/A	569	N/A		

LEGEND: AA-B-C-D-E

AA:	Exposure	C = control (no exposure), W = water exposure, SW = salt water exposure, CPS = CPS exposure
B:	Temperature of exposure	
C:	Plate geometry	F = flat plate, R = round plate
D:	Prestress	0 = no prestress, L = low prestress (9.8 kN), H = high prestress (19.7 kN)
E:	Sample #	1 = first sample, 2 = second sample, 3 = third sample 1*=uptake validation specimen

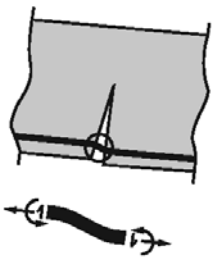

Figure 1. Dowel action

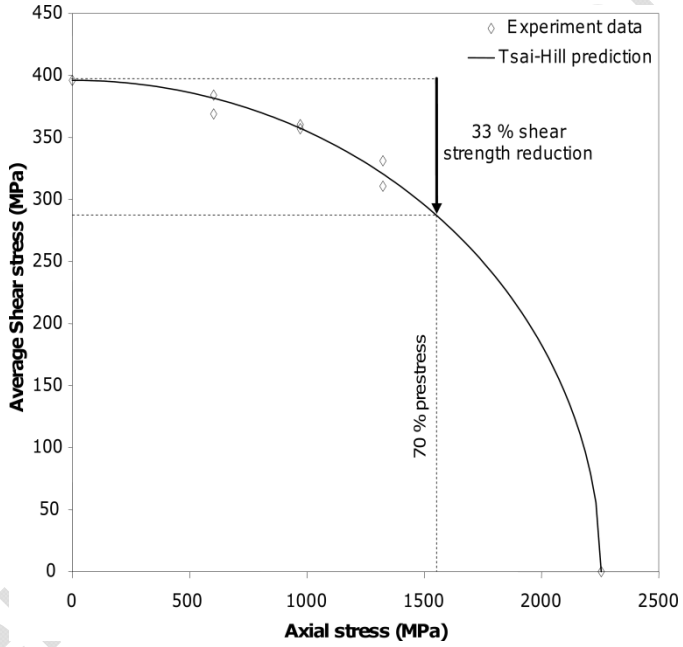

Figure 2. Relationship between shear stress and axial stress at failure in tests of CFRP tendons by Park and Naaman [4]

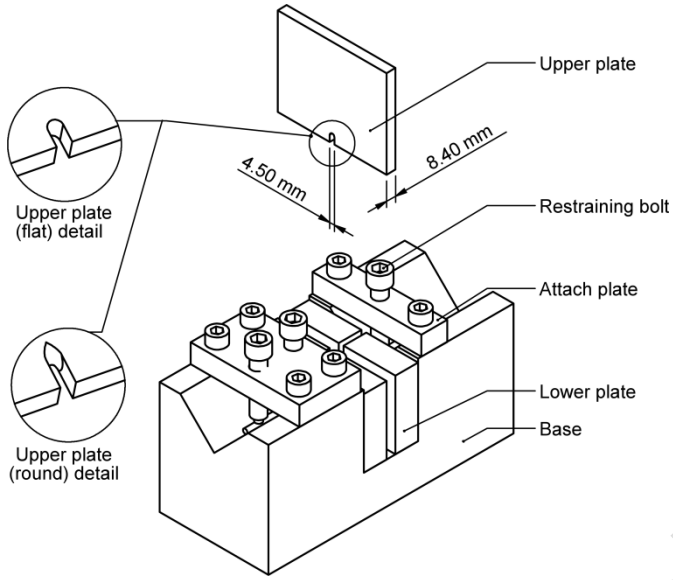

Figure 3. Double shear test rig

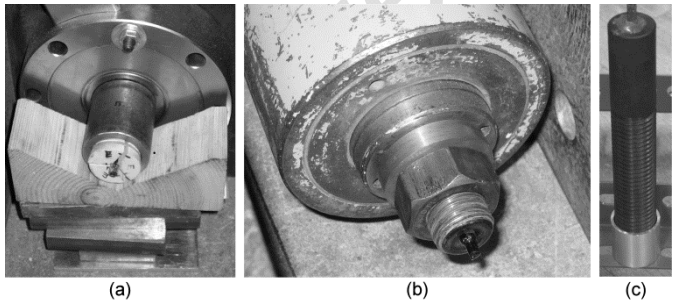

Figure 4. Tendon anchorages (a) mechanical anchor and (b) potted anchor (c) photo of potted anchor

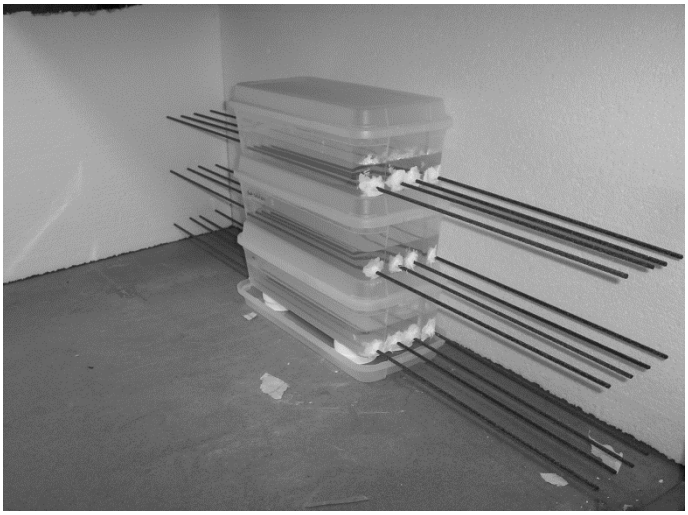

Figure 5. Exposed specimens before being placed in oven at 60°C

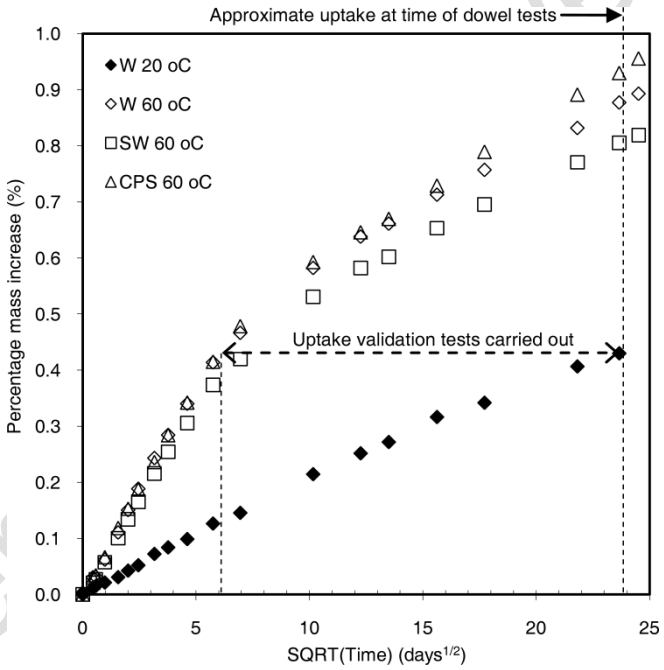

Figure 6. Solution uptake in specimens tested

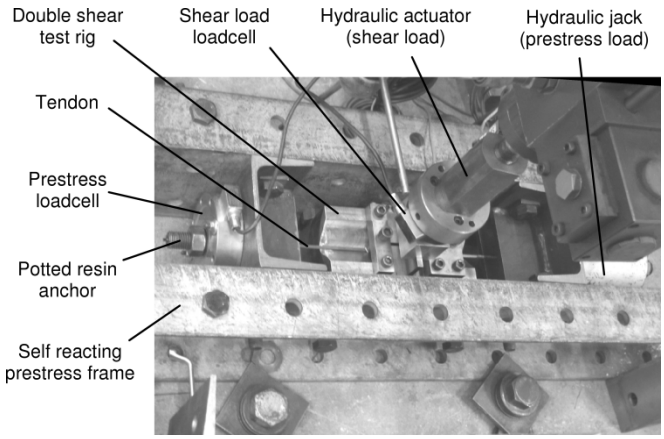

Figure 7. Shear loading support frame, shear load actuator and prestress rig (view from above)

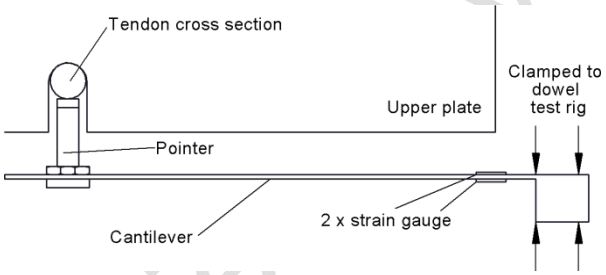

Figure 8. Cantilever displacement transducer

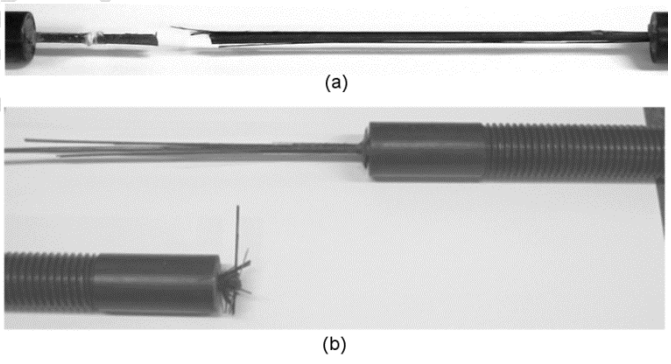

Figure 9. Pure axial failure modes (a) free length failure in SW specimen and (b) anchorage failure in control specimen

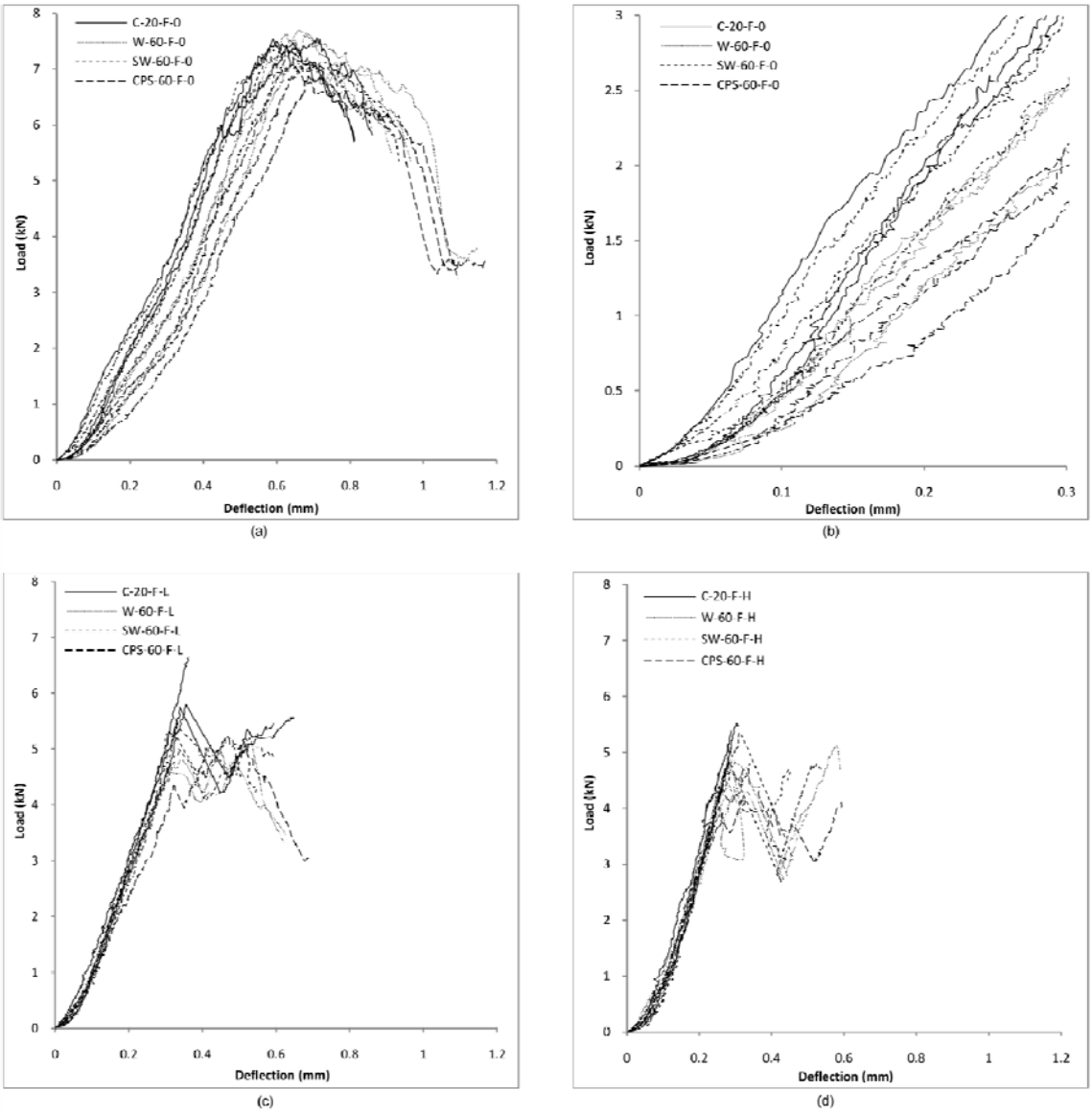

Figure 10. Load/deflection behaviour for (a) no prestress (b) no prestress - expanded view of behaviour at low deflections (c) low prestress and (d) high prestress flat plate tests

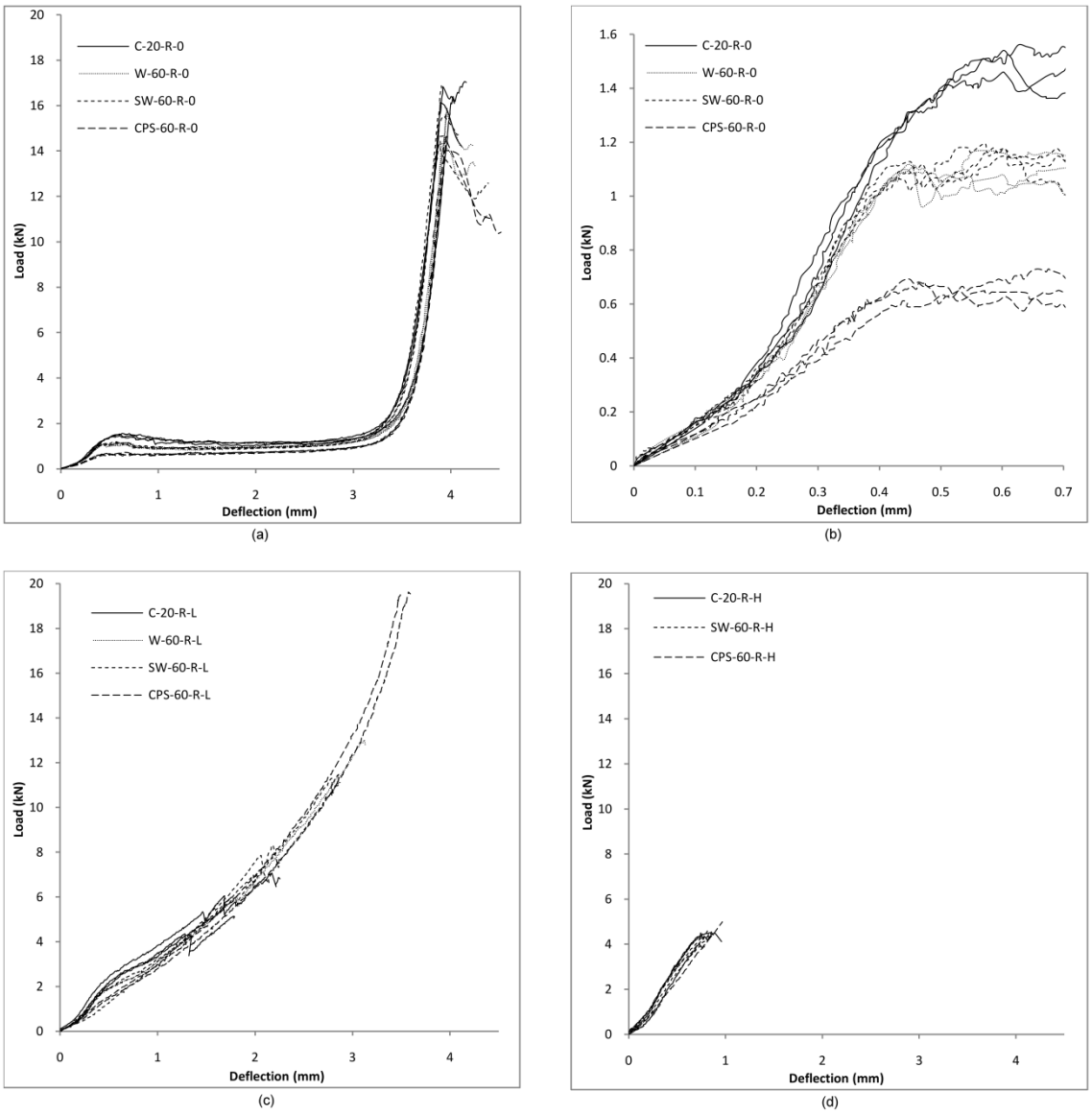

Figure 11. Load/deflection behaviour for (a) no prestress (b) no prestress - expanded view of behaviour at low deflections (c) low prestress and (d) high prestress round plate tests

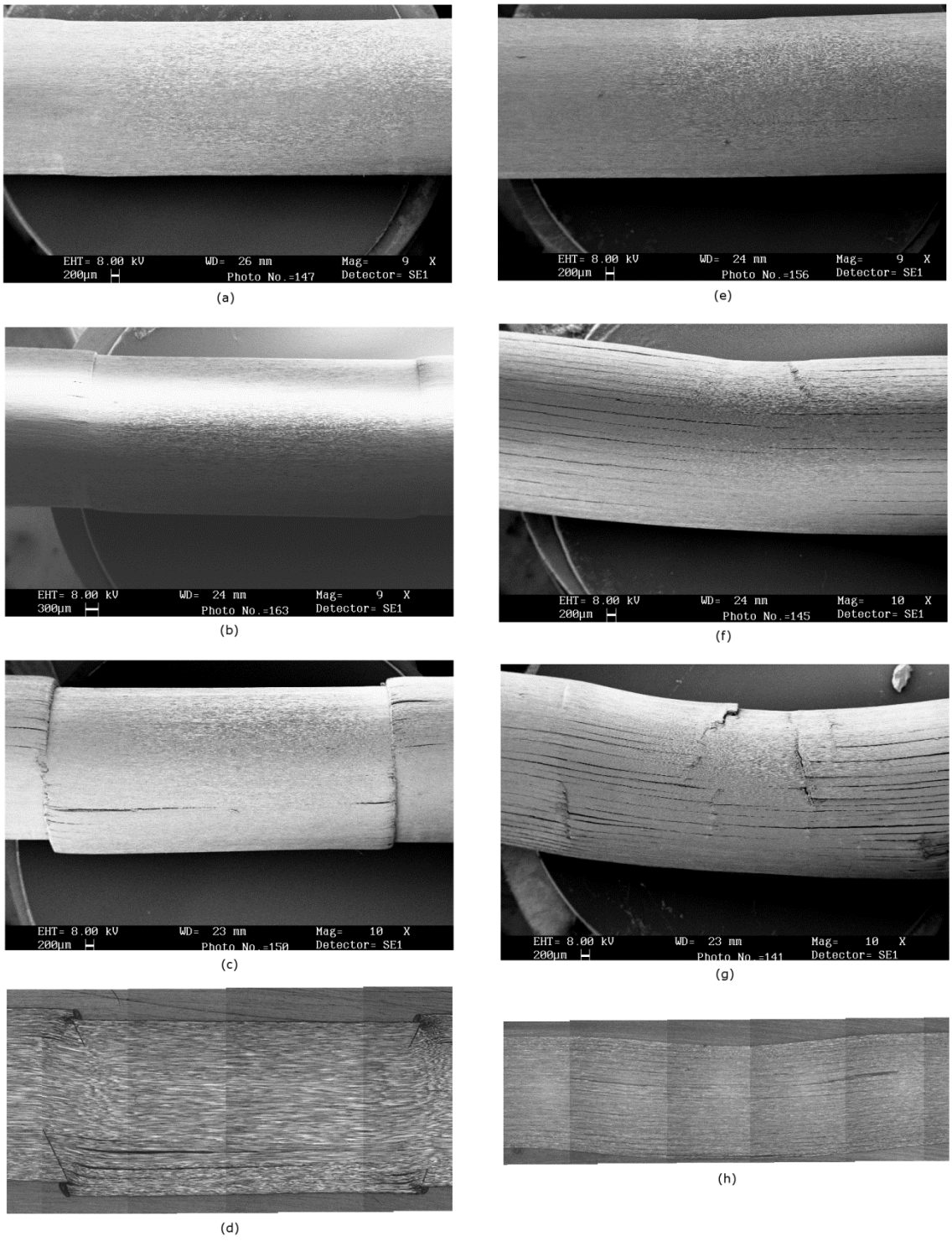

Figure 12. Flat plates - SEM images after loading to and unloading from (a) 2.9kN (b) 5.9kN (c) 7.6 kN and (d) associated optical image for 7.6 kN specimen, and round plates - SEM images after loading to and unloading from (e) 1.7 kN and 0.7 mm (f) 1.7 kN and 3 mm and (g) 16.1 kN and (h) associated optical image for 16.1 kN specimen

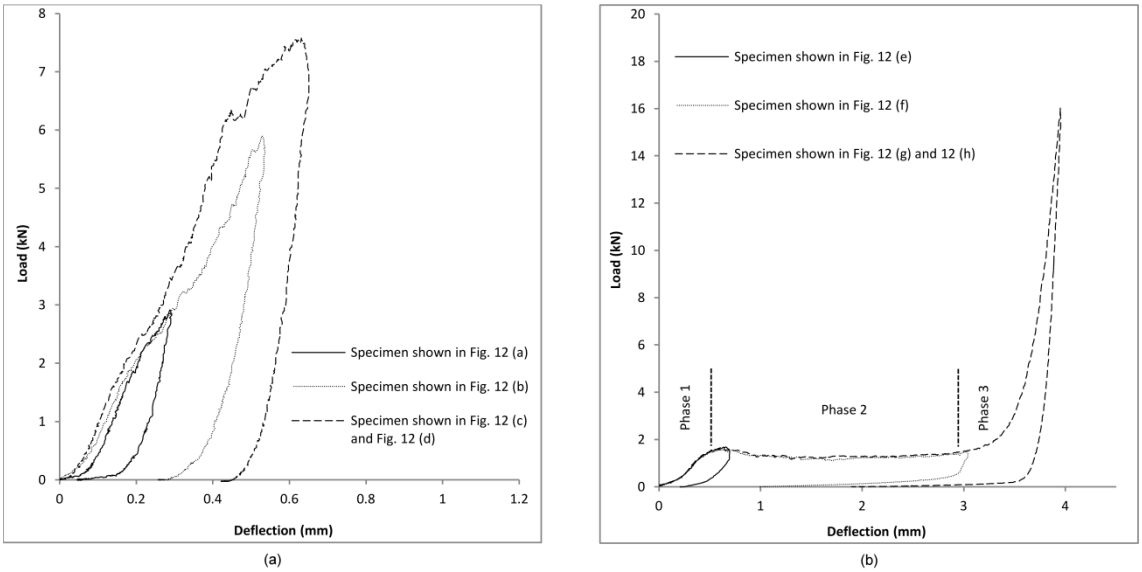

Figure 13. Load deflection curves for partial loading tests using (a) flat plates and (b) round plates

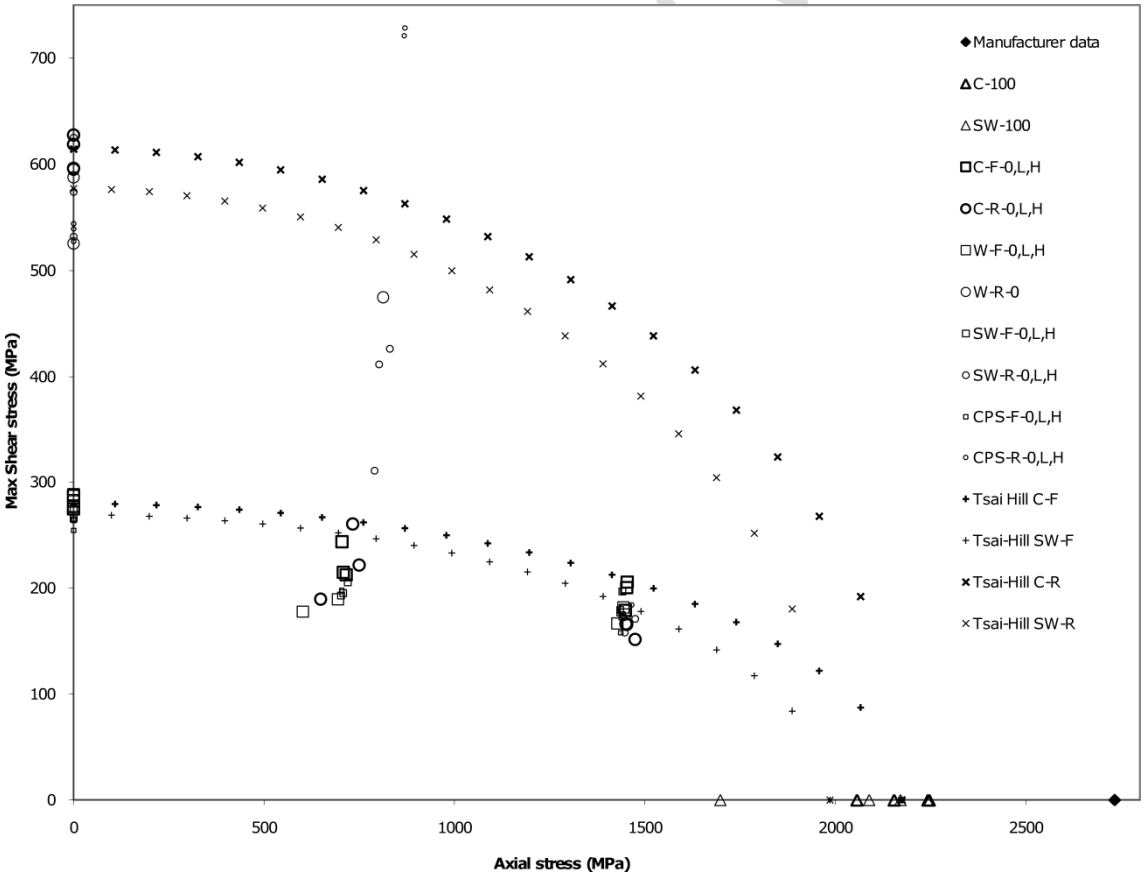

Figure 14. Dowel test failure envelope